THE VORTEX MERGER FACTOR IN AIRCRAFT WAKE TURBULENCE

Miroslav Mokry
Institute for Aerospace Research, NRC
Ottawa, Canada

Abstract

Vortex merger is studied within the context of two-dimensional discrete vortex sheets and demonstrated on two equally oriented circular vortices and aircraft tip and flap vortices. It is confirmed that, depending on the wing load distribution, the latter may or may not coalesce into a single counter-rotating pair. The interaction of a vortex with an equally oriented shear layer, governed by the same physical principle, suggests a possible intensification of an aircraft vortex in cross-wind shear.

Symbols

AR	wing aspect ratio
a	vortex circuit radius
b	wing span
C	oriented vortex sheet
C_L	lift coefficient
C_l	sectional lift coefficient
c	chord length
d	downstream distance
f	Cauchy density
g	circulation around grid point
i	imaginary unit
j	circle index
k	Gaussian distribution parameter
L	angular momentum
n	number of concentric circles
R	vortex patch radius
r	radial coordinate
S	wing reference area
s	vortex centre separation distance
U	aircraft velocity
v_n	normal velocity
v_t	tangential velocity
v_θ	azimuthal velocity
w	complex velocity
x	spanwise (horizontal) coordinate
y	vertical coordinate
z	complex coordinate (observation point)
Γ	circulation
γ	vortex line density
ν	normal angle, Fig.2
τ	pseudotime
ζ	complex coordinate (contour point)
θ	polar angle
ρ	fluid density
ω	vorticity

Superscripts

$+$	value to the left of C
$-$	value to the right of C
$*$	complex conjugate

Subscripts

cr	critical
eff	effective
j, k	grid point
0	constant value

Introduction

By definition, two-dimensional merger occurs when two vortices of the same sign and within a certain critical distance of each other mix a substantial portion of their core vorticity to become a single vortex. A beautiful experimental example has been given by Meunier and Leweke [1]. Their result, reproduced here in Fig.1, shows the merging of two co-rotating planar vortices, having the same circulation.

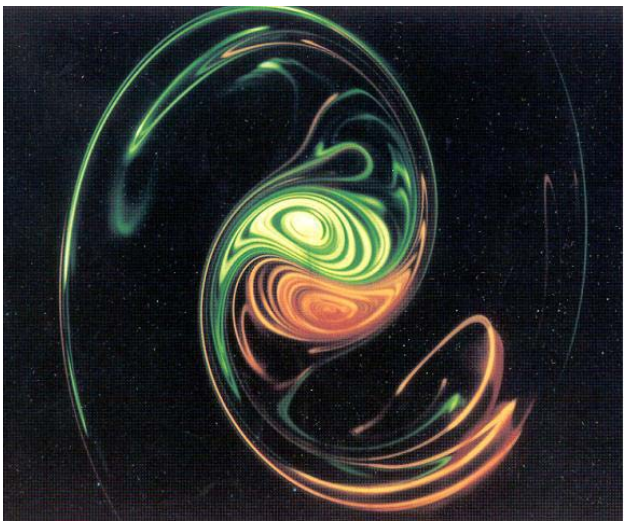


Fig.1 Merging of a pair of co-rotating vortices (courtesy of Meunier and Leweke, IRPHE Marseille[1]).

https://doi.org/10.1017/S0001924000000531 Published online by Cambridge University Press

The vortex pair was generated in water at the sharpened edges of two flat plates, moved impulsively from rest. Flow visualization was implemented using two different fluorescent dyes, illuminated by a laser sheet perpendicular to the vortex axes. The investigators describe several stages of the process: the rotation of the vortices about each other due to self-induction, increase of the vortex cores by diffusion, distortion and attraction with an increased spin around each other, and merger into one single vortex.

The salient feature of this interaction is the strain induced by two closely spaced vortices on each other: two patches of equally oriented vorticity interact in such a way that the inner portions rotate about each other faster than the outer portions. The reduction of energy in the extended portions of the vortices is balanced its increase in the attracted inner portions. The process towards equilibrium, characterized by the minimum enstrophy compatible with a given energy [2], consists of the simultaneous filamentation and consolidation [3].

It has been widely recognized that merger of vortices plays a central role in cascading energy towards larger scales and, also, cascading enstrophy to smaller scales [4][5]. Mergers of vortices have been observed in large-scale atmospheric [6] and oceanic flows [7], but also in subscale laboratory experiments with magnetically confined columns of electrons [8]-[12]. This magneto-electrical analog is based on the observation [8] that the 2D drift Poisson equations for the evolution of the electron column are isomorphic to the 2D Euler equations for an inviscid fluid of uniform density. Thus, the electron columns evolve the same as vortex tubes.

Discrete Vortex Sheet Method

In this paper, the method of discrete vortex sheets [13] is used to provide numerical simulations of various types of vortex mergers. An advantage of this method is that it conserves vorticity and allows the solution to develop over relatively large times.

In the cross-flow (Trefftz) plane, the complex velocity induced by the vortex sheet C is represented by the line distribution of vorticity

$$w(z) = \int_C \frac{i\gamma(\zeta)}{2\pi(\zeta - z)} |d\zeta| \qquad (1a)$$

where $|d\zeta|$ is the arc length element of C. The real-valued vortex density γ is positive if the vortex sheet element turns flow counterclockwise and negative if it turns flow clockwise. An alternative form of Eq.(1a) is the Cauchy-type integral

$$w(z) = \frac{1}{2\pi i} \int_C \frac{f(\zeta)}{\zeta - z} d\zeta \qquad (1b)$$

where

$$f(\zeta) = i\gamma(\zeta) e^{-i\nu(\zeta)} \qquad (2)$$

is the complex density function defined on C and ν is the angle between the normal to C and the real axis, see Fig.2. Since in the complex-variable treatment $z = x + iy$, we denote the cross-flow coordinates x and y instead of the more common y and z.

In accordance with the Plemelj formula [14]

$$w^+(\zeta) - w^-(\zeta) = f(\zeta) \qquad (3)$$

where the superscripts $+$ and $-$ designate the limiting values of w to the left and right of C, respectively. Along C, as may be verified from appropriate velocity triangles,

$$w(\zeta) = [v_n(\zeta) - iv_t(\zeta)]\, e^{-i\nu(\zeta)} \qquad (4)$$

where v_n and v_t are the normal and tangential velocities respectively. Using Eqs.(2-4), it follows for the differences of normal and tangential velocities across the sheet

$$v_n^+(\zeta) - v_n^-(\zeta) = 0 \qquad (5a)$$

$$v_t^+(\zeta) - v_t^-(\zeta) = -\gamma(\zeta) \qquad (5b)$$

The time evolution of the discretized vortex sheet C is investigated in the Lagrangian context, by integrating

$$\frac{dz}{d\tau} = w^*(z) \qquad (6)$$

in pseudotime τ. The right-hand side term of Eq.(6) is the complex conjugate of the principal value of the integral of Eq.(1b).

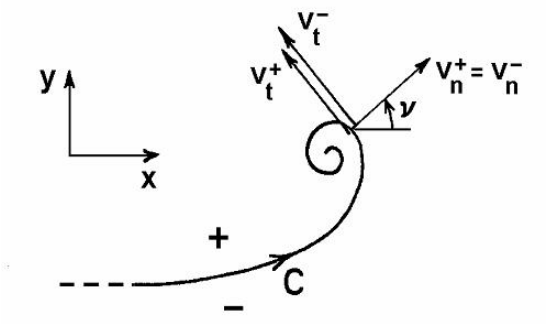


Fig.2 Discrete vortex sheet representation.

https://doi.org/10.1017/S0001924000000531 Published online by Cambridge University Press

The solution is advanced in finite time increments $\Delta\tau$ using the second-order Runge-Kutta method. The trial step to the midpoint of the time interval is implemented as

$$z_1(\tau + \tfrac{1}{2}\Delta\tau) = z(\tau) + w^*[z(\tau)]\,\tfrac{1}{2}\Delta\tau \qquad (7a)$$

and the actual step across the whole interval as

$$z(\tau + \Delta\tau) = z(\tau) + w^*[z_1(\tau + \tfrac{1}{2}\Delta\tau)]\,\Delta\tau \qquad (7b)$$

Local conservation of vorticity is enforced by the condition

$$\gamma(\zeta)|d\zeta| = \text{constant} \qquad (8)$$

Accordingly, when the vortex segment elongates, its density decreases, and when it contracts, its density increases. (This process is not to be confused with 3D stretching, which changes the vorticity content inside a vortex tube.)

Because at later times the highly elongated vortex line segments tend to intersect, it is appropriate to present the global flow features in terms of velocity vectors mapped over the vorticity field. Velocity components u, v are evaluated from Eq.(1a) on a rectangular mesh j, k. The vorticity is calculated by the circulation method [15]:

$$\omega_{j,k} = \frac{g_{j,k}}{4\Delta x \Delta y} \qquad (9)$$

where

$$\Delta x = x_{j+1} - x_j \quad \text{and} \quad \Delta y = y_{k+1} - y_k \qquad (10)$$

and

$$\begin{aligned} g_{j,k} =& \tfrac{1}{2}\Delta x[(u_{j+1,k+1} + 2u_{j,k+1} + u_{j-1,k+1}) \\ & - (u_{j-1,k-1} + 2u_{j,k-1} + u_{j+1,k-1})] \\ & + \tfrac{1}{2}\Delta y[(v_{j+1,k-1} + 2v_{j+1,k} + v_{j+1,k+1}) \\ & - (v_{j-1,k+1} + 2v_{j-1,k} + v_{j-1,k-1})] \end{aligned} \qquad (11)$$

In this post-processing, the selection of the mesh size plays an important role. If it is too coarse, the local flow details are not resolved; if it is too refined, the vortex sheets re-appear on the potential-flow background

Interaction of Vortex Patches

There has been a large amount of research devoted to vortex merger with particular emphasis on the case of two identical vortices (symmetric merger) [16][17]. The prototype of a two-dimensional vortex is a vortex patch, defined as a connected, finite region of rotational fluid surrounded by fluid that is irrotational. The patch can be also viewed as the perpendicular section of an infinitely long rectilinear vortex tube whose vorticity distribution is invariant along the length of the tube [18]. If the region is circular of radius R and contains constant vorticity, $\omega = \omega_0$, the vortex patch models a Rankine vortex, with the azimuthal velocity [19]

$$v_\theta = \begin{cases} \dfrac{\Gamma}{2\pi r}, & r > R \\ \dfrac{\Gamma r}{2\pi R^2}, & r < R \end{cases} \qquad (12)$$

where

$$\Gamma = \pi R^2 \omega_0 \qquad (13)$$

Outside the patch, the flow is irrotational, equivalent to that generated by a single point vortex of strength Γ located at the centre of the circular patch. The patch itself rotates like a solid disk with angular velocity $\omega_0/2$.

Denoting by ρ the fluid density, the angular momentum of a circular patch of radius R is obtained as

$$L = 2\pi\rho \int_0^R v_\theta r^2 dr \qquad (14)$$

Substituting from Eqs.(12) and (13)

$$L = \frac{\pi}{4}\rho R^4 \omega_0 \qquad (15)$$

The earlier numerical studies of vortex patch evolutions used vortex-in cell methods [20][21] and contour dynamics [22]-[24]. In the discrete vortex sheet method, employed in this paper, the circular vortex patch is approximated by a set of equidistant concentric circles with the vortex density initialized as $\gamma = \gamma_0$. The contour coordinate of the circle C of radius a, centered at the origin, is

$$\zeta = a e^{i\nu} \qquad (16)$$

where $\nu = \nu(\zeta) = \theta$ is the polar angle. From Eqs.(2) and (16)

$$f(\zeta) = i\gamma_0 e^{-i\nu} = i\gamma_0 \frac{a}{\zeta} \qquad (17)$$

and, substituting in Eq.(1b),

$$w(z) = i\gamma_0 a \frac{1}{2\pi i} \int_C \frac{1}{\zeta} \frac{d\zeta}{\zeta - z}$$

Since the analytic continuation of $1/\zeta$ is the function $1/z$, nonsingular in the exterior domain $|z| > a$ and

https://doi.org/10.1017/S0001924000000531 Published online by Cambridge University Press

vanishing at infinity, the value of the above Cauchy type integral is

$$w(z) = \begin{cases} -a\gamma_0 \dfrac{i}{z}, & |z| > a \\ 0, & |z| < a \end{cases} \tag{18}$$

This result shows that outside the circle, the flow field is identical with that generated by a point vortex of strength $2\pi a\gamma_0$, located at the centre of the circle. Inside, there is no flow. From Eq.(18) it follows for the azimuthal velocity as function of the distance r from the centre

$$v_\theta = \begin{cases} \gamma_0 \dfrac{a}{r}, & r > a \\ 0, & r < a \end{cases} \tag{19}$$

The jump discontinuity at $r = a$ is consistent with that described by Eq.(5b).

In order to approximate a uniform-vorticity patch, n concentric circles of radii

$$a = R\,\frac{j}{n}, \qquad j = 1, \cdots, n \tag{20}$$

and constant density γ_0 are used. Accordingly, the total circulation is

$$\Gamma = 2\pi R\gamma_0 \sum_{j=1}^{n} \frac{j}{n} = (n+1)\pi R\gamma_0 \tag{21}$$

Comparing Eqs.(13) and (21) we obtain the relationship between the vortex line density and the vorticity inside the patch

$$\gamma_0 = \frac{R\omega_0}{n+1} \tag{22}$$

This relationship establishes the correspondence of velocities outside the patch, but not inside. From Eqs.(14),(19),(20) and (22), the angular momentum of the patch represented by n equidistant vorticity circuits is

$$L = \frac{n-1}{n}\,\frac{\pi}{4}\,\rho R^4\omega_0 \tag{23}$$

It is zero for a single circuit, $n = 1$, and tends to the correct value given by Eq.(15) as $n \to \infty$.

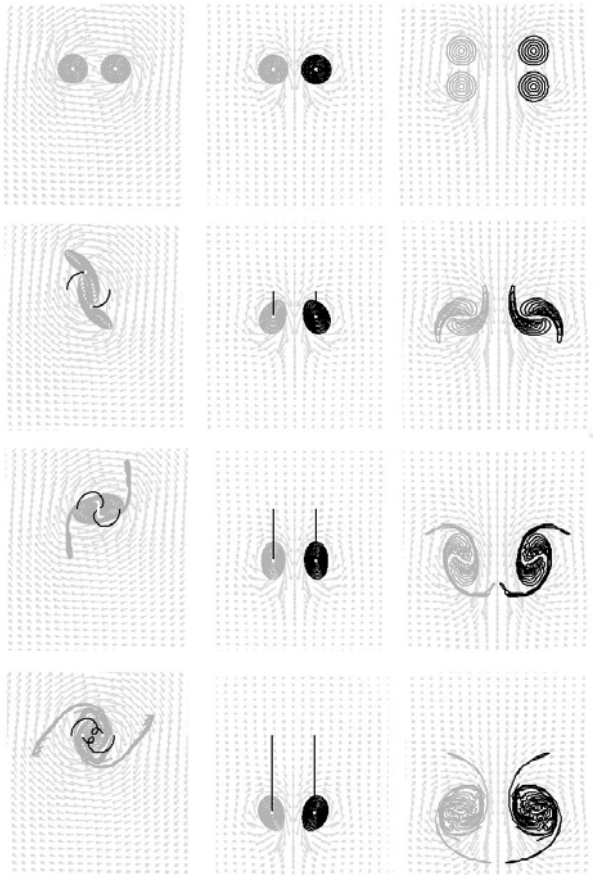
Following the discussion in Ref.[25], each vortex circuit of radius a is assumed to represent the vorticity of an annular region $a - R/(2n) < r < a + R/(2n)$. Accordingly, the "effective" patch radius is

$$R_{\text{eff}} = R\left(1 + \frac{1}{2n}\right) \tag{24}$$

The example in Fig.3a shows the evolution of two equally oriented patches, represented by 10 concentric circles each. In the sequence of constant time increments, we observe the merger of the two vortices into one. The appearance of two periferal filaments (halo arms) resembles the experimental result in Fig.1. The absence of roll-up of the filament ends is ascribed to the stabilizing effect of straining induced by the compound vortex [26][27].

As shown in Fig.3b, the counter-rotating (dipolar) vortices do not merge. They descend by self-induction while undergoing deformations due to mutual strain. The observed geometrical phases suggest the origins of the three-dimensional long-wavelength instability [28][29].

Merger of two counter-rotating vortex pairs is shown in Fig.3c. It illustrates in a simplified fashion how wing tip vortices may merge with flap vortices. The interaction pattern depends of course on the particular configuration, separation distances and vortex strengths [30].



a) co-rotating b) counter-rotating c) 2 pairs

Fig.3 Evolution of circular vortex patches in constant-time increments.

https://doi.org/10.1017/S0001924000000531 Published online by Cambridge University Press

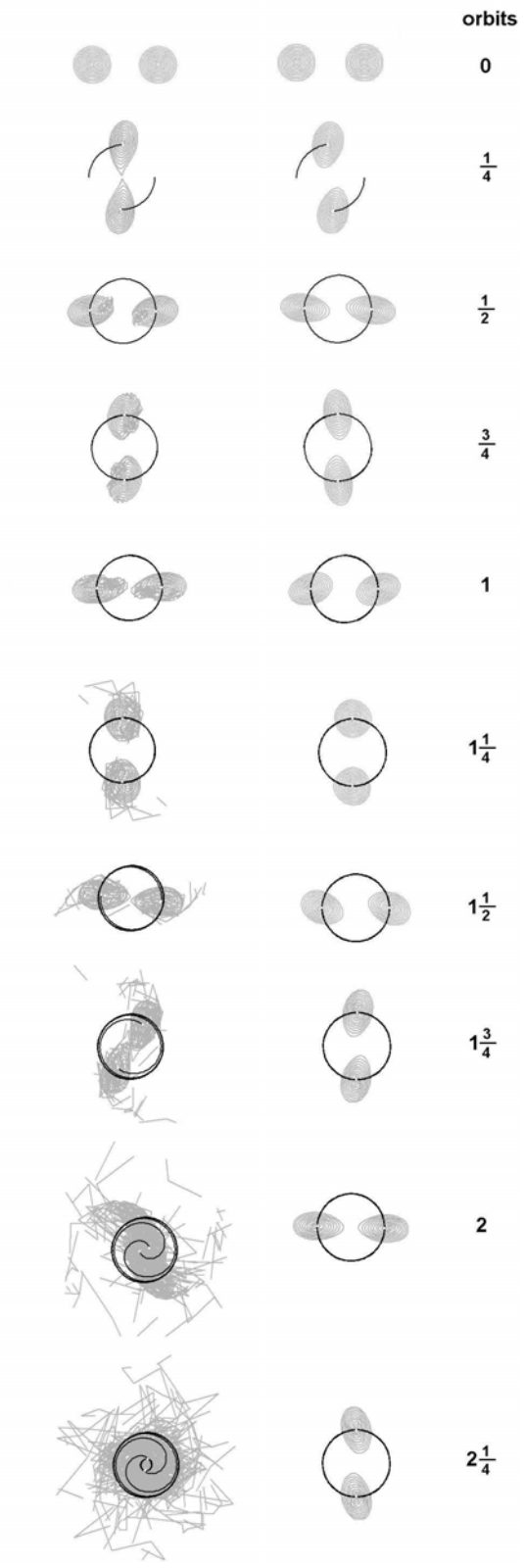
From the previous examples it might appear that merger is a natural outcome of the interaction of equally oriented vortices. Indeed, from the very start of the process, the velocity is zero at the global vorticity centroid and the far field is that of a single vortex. However, the transition to a monopole configuration is subject to constraints imposed by the conservation of angular momentum and energy [31]. For example, if two very distant, identical vortices were brought to coincide, the (excess) kinetic energy of the system would double [3]. In an isolated system, this energy increase is clearly not possible.

The determination of the critical separation distance s_{cr} below which the merger takes place and above which it does not, has proven analytically intractable [10]. The principal difficulty is that merger does not come about until the vortex patches, subjected to mutual strain, become sufficiently distorted from their circular shapes to come into contact. One has to therefore rely upon numerical simulation or experiment. Presumably, the key to solving this inviscid-flow problem is the limit as the number of vortex orbits tends to infinity.

Earlier numerical analyses [4][5], confined to a smaller number of orbits, proposed $s_{\mathrm{cr}}/R = 3.3 \pm 0.2$, see Ref. [32]. However, electron plasma vortices were found to merge at separation distances as high $s/R = 3.6$ because, due to negligible dissipation, up to 10^4 vortex orbits could be produced [9]. In contrast, experimental evidence in the fluid-dynamics domain suggests that merger of a co-rotating vortex pair occurs typically within one orbital period [33][34].

One question that still remains unanswered is the quantification of the amounts of vorticity imparted to filamentary structures during the merger process [17]. To address this issue, examples in Fig.4 are given to show the interactions of vortex patches, separated just below and above the critical distance, as determined by the discrete vortex method. In these cases each patch was represented by 10 circular contours with a constant, negative vortex density.

For $s < s_{\mathrm{cr}}$, Fig.4a, the centroids of the patches describe near-circular orbit trajectories until the extended innermost portions touch to initiate a short duration rollup, and the filamentation process of the outer portions takes hold. Eventually, the patches merge together to form a single vortex surrounded by a sea of filamentary debris [35]. Measured by the loss of globally conserved quantities to filaments and small-scale structures, such a merger would be less efficient than those shown earlier in Figs.1 and 3a.



a) $s/R_{\mathrm{eff}} = 3.43$ b) $s/R_{\mathrm{eff}} = 3.52$

Fig.4 Merger and non-merger of circular vortex patches near critical distance.

https://doi.org/10.1017/S0001924000000531 Published online by Cambridge University Press

Experimentally, the fraction of the total vorticity found in the compound vortex is between 70% and 90% [11], but seldom less than 55% [17]. One can conjecture that if the merger took place just at the critical distance, the compound vortex would contain 50% of the total vorticity (equivalent to a single patch) and the other 50% would be advected away (dispersed). In other words, the merger efficiency would be zero.

For $s > s_{cr}$, Fig.4b, the circular patches do not make contact and continue to rotate around their mutual centre of vorticity at approximately the same rate as point vortices with the with the same circulation. The paths of the centroids are perfectly circular, however, the patches pulsate through several states as they rotate about each other. Eventually, the accumulated numerical errors would make the representing vorticity contours Helmholtz-unstable and the patches would merge even in this case.

Although the symmetric vortex merger is rare, the processes described, such as filamentation and consolidation, constitute the essential growth mechanism of localized regions of vorticity in 2D flows [36][37]. The outcome, particularly when the two interacting vortices have vastly different sizes and circulations, may of course be quite different [10][35][36].

Wake Vortices

As discussed in Refs.[38]-[40], the evolution of the vortices in the wake of an aircraft can be divided into the following zones:
- the near field, usually no more than one wing span downstream, in which several smaller vortices spring off the wing tips, edges of flaps, wing-fuselage junctions, and so on,
- the "extended" near field, typically up to 12 wing spans downstream, in which the smaller vortices merge into a pair of counter-rotating vortices,
- the mid field, characterized by a steady condition of the vortex pair, and
- the far field where the wake vortices become unstable and the decay of circulation sets in.

The near-field vortex evolution is demonstrated using the recently published [41] experimental data of the DLR-F11 model in the take-off configuration. The test was conducted on a half model in the 3.25 x 2.8 m^2 working section of the DNW-NWB low speed wind tunnel in Braunschweig. The wing-section lateral coordinates, chord lengths and lift coefficients are given in Table 1.

Table 1 DLR-F11 wing load distribution (courtesy of DLR).

b =2.8 m (full model)
$AR = 9.23$
C_L =1.76
U =60.0 m/s

x/b	c/b	C_l
0.075	0.17108	1.4232
0.144	0.13664	1.8522
0.225	0.11574	2.1512
0.272	0.10362	2.0827
0.341	0.08582	2.1719
0.358	0.08144	2.0679
0.376	0.07679	1.7561
0.409	0.06828	1.5304
0.446	0.05874	1.3347
0.482	0.04945	0.8070

The wing-section circulation is by Joukowski's theorem

$$\Gamma(x) = \tfrac{1}{2} U c(x) C_l(x) \tag{25}$$

Here U denotes the wind speed; c and C_l are the wing-section chord length and lift coefficient respectively. The non-dimensional vortex density is obtained as [13]

$$\begin{aligned} \gamma(x) &= -\frac{\pi}{U}\frac{b^2}{SC_L}\frac{d\Gamma(x)}{dx} \\ &= -\frac{\pi}{2}\frac{AR}{C_L}\frac{d}{dx}[c(x)C_l(x)] \end{aligned} \tag{26}$$

where b is the wing span, S is the reference area, and

$$C_L = \int_{-b/2}^{b/2} \frac{c(x)C_l(x)}{S} dx \tag{27}$$

is the overall lift coefficient.

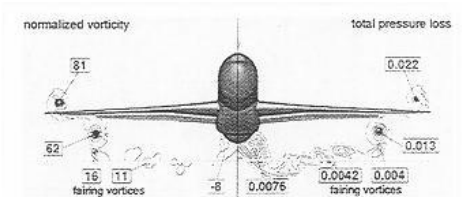
The solution is advanced in the length-dimensioned pseudotime τ, related to the downstream distance as [13]

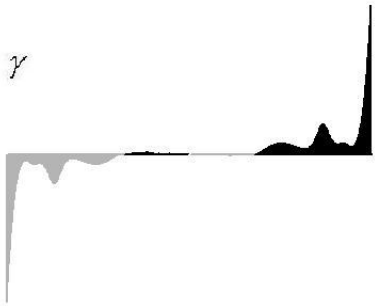
$$d = \frac{\pi AR}{C_L}\tau \tag{28}$$

From the data given in Table 1, $d \approx 16.5\tau$.

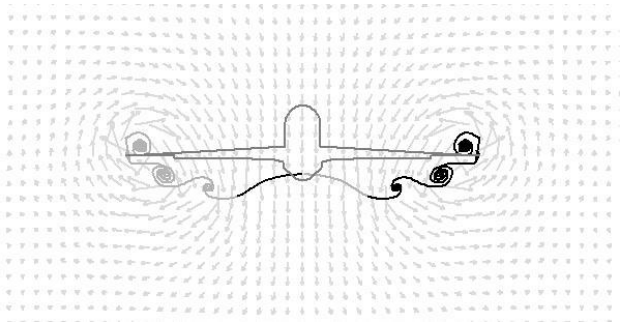
Contours of the normalized velocity and total pressure, obtained by traversing a five-hole probe in the cross-flow plane at the distance of 0.5 wing spans downstream of the trailing edge of the wing, are shown in Fig.5a.

https://doi.org/10.1017/S0001924000000531 Published online by Cambridge University Press

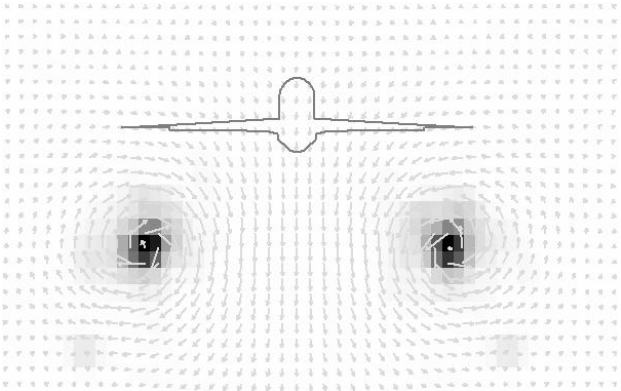




b) initial vortex density, $d/b = 0.0$



c) discrete vortex sheet simulation, $d/b = 0.5$



d) discrete vortex sheet simulation, $d/b = 10.0$

Fig.5 Vortices behind a take-off configuration of the DLR-F11 model, b =2.8 m, AR =9.23 U =60 m/s, C_L =1.76.

The initial vortex density, evaluated from Eqs.(26) and (27), is plotted in Fig.5b. The positive density, turning the flow anticlockwise, is plotted in black and the negative density, turning the flow clockwise, is plotted in grey.

The discrete vortex sheet simulation used 480 segments and the time step τ/b =0.0001. Elongation of vortex segments is the general trend, with the exception of those near the maxima of $|\gamma|$, where a local contraction may take place prior to rollup [13].

The vortex sheet and the velocity vector map at τ/b =0.03 (corresponds to $d/b \approx$0.5) are shown in Fig.5c. The morphologies of the vortices, observed experimentally, Fig.5a, and computationally, Fig.5c, are very similar at this near-field station. Although the centres of the port and starboard vorticity are convected downward from the very start, the wing tip vortices at this early rollup stage are found above the wing. This is attributed to the fact that prior to merger the wing tip and flap vortices rotate about each other.

The computation can of course be continued. The result in Fig.5d corresponds to an extended near-field location d/b =10 and is plotted as the velocity vector matrix over the distribution of $|\omega|$. It shows the wing tip and flap vortices already merged into a single couple of counter-rotating vortices. The origins of the stray vortices near the left and right lower corners of Fig.5d are the wing-fuselage junctions. As may be verified from the vortex density plot in Fig.5b, they are oppositely signed to the main vortices, and hence are not merged.

Merger of vortices behind transport aircraft models has been investigated both in long wind tunnel test sections [38][39][42]-[44] and towing tank facilities [40][45]-[47], to acknowledge just a few. Both passive devices, altering the circulation distribution, and active devices, promoting an earlier demise of the generated vortices, have been proposed.

Recently, Graham at al.[42][48] have shown that wing vortex merger can be suppressed using a 'notched' planform design. This type of wing generates a spanwise lift distribution with a local minimum between the regions contributing to the flap and tip vortices. The counter-signed vortex associated with this minimum keeps the flap and tip vortices apart, preventing their merger and reducing substantially the rolling moment on a following aircraft.

https://doi.org/10.1017/S0001924000000531 Published online by Cambridge University Press

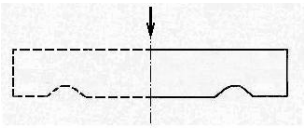


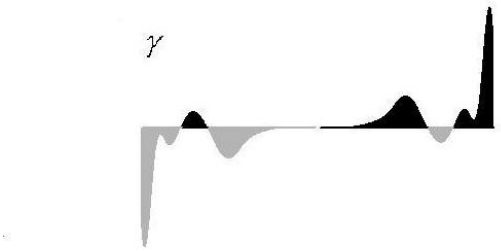
Fig.6 Notched wing.

The planform of the notched wing is shown in Fig.6. The spanwise lift distribution, obtained from the lifting line theory, is given in Table 2. From Eq.(28), the relationship between the pseudotime and downstream distance is in this case $d \approx 43.8\tau$.

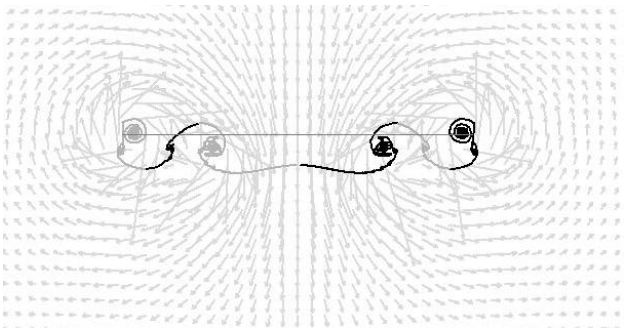
Table 2 Notched wing load distribution (based on [42]).

b =0.6 m (entire wing)		
$AR = 6$		
C_L =0.43		
U =0.534 m/s		
x/b	c/b	C_l
0.050	0.175	1.83
0.100	0.175	1.79
0.150	0.175	1.75
0.200	0.175	1.64
0.225	0.175	1.52
0.250	0.150	1.55
0.300	0.128	1.35
0.350	0.150	1.27
0.375	0.170	1.22
0.400	0.170	1.22
0.450	0.170	0.98
0.475	0.170	0.78
0.500	0.170	0.00

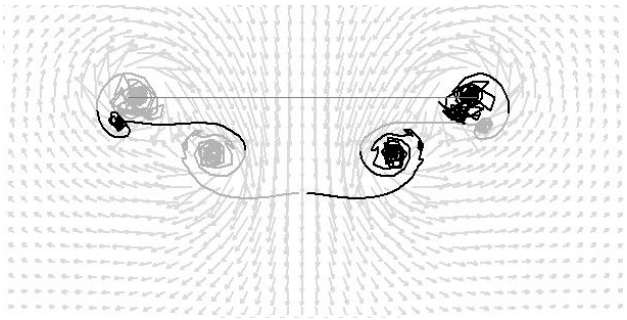
The vortex density function of the initial trailing sheet, calculated from Eq.(26), is shown in Fig.7a. There are several local extrema, giving rise to subsequent roll-ups. Most notable are those containing the vorticity oppositely signed to that prevalent on each side of the wing (the grey region embedded in the black region and vice versa). Figs.7b-d show the vortex formations, calculated by dividing the vortex sheet into 960 segments and using the pseudotime step τ/b =0.0001. In the near-field region investigated, the counter-signed vortices rotate around the wing tip vortices, preventing them from merging with the flap vortices. The extended near field result in Fig.7d shows that the tip and flap vortices remain distinct in agreement with earlier water tunnel tests of Ref.[48].



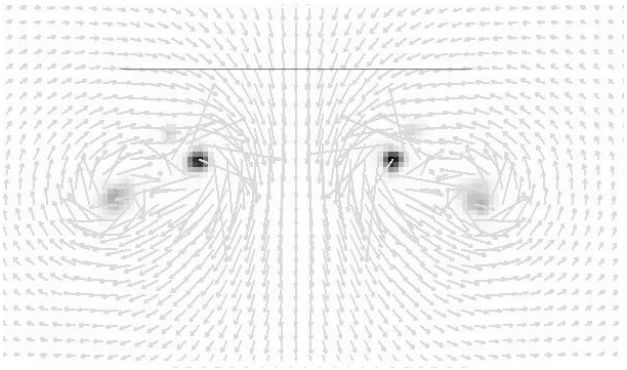
a) initial vortex density, $d/b = 0.0$



b) discrete vortex sheet simulation, $d/b = 0.6$



c) discrete vortex sheet simulation, $d/b = 2.0$



d) discrete vortex sheet simulation, $d/b = 10.0$

Fig.7 Vortices behind the notched wing (AR =6.0, C_L =0.43).

https://doi.org/10.1017/S0001924000000531 Published online by Cambridge University Press

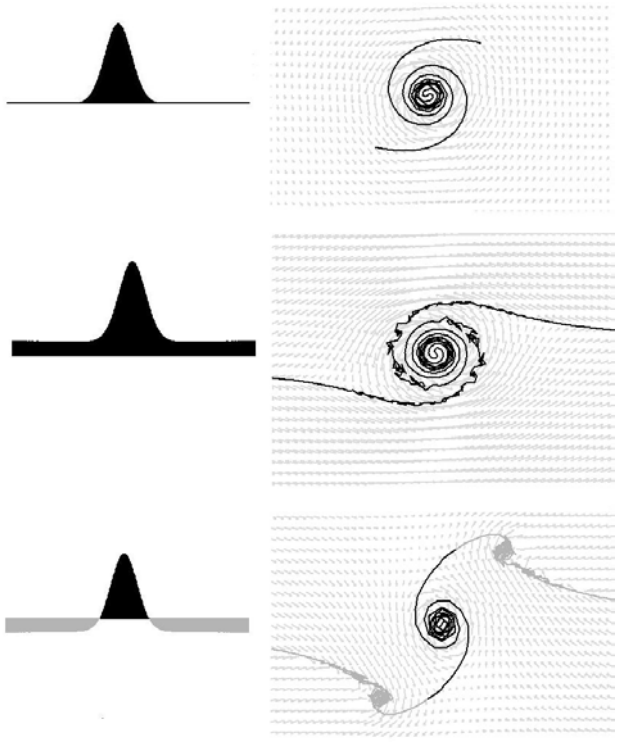
Vortices in Shear

Conceivably, the interactions of the equally signed or oppositely signed vorticity are not necessarily limited to patches, isolated vortices or trailing shear layers. Similar patterns can be also observed in background shear [12] or other types of flow containing vorticity.

The following example was chosen to show the evolution of an isolated vortex in ambient shear. The first case concerns an isolated vortex, initialized by the straight line $y = 0$ with the vortex density

$$\gamma = \frac{k}{\sqrt{\pi}} \exp(-k^2 x^2) + \gamma_0, \quad -\infty < x < \infty \qquad (29)$$

By selecting k we set the maximum value of the Gaussian term; in the limit $k \to \infty$ it tends to the Dirac delta function. In our specific example $k = 5$ is chosen, resulting in $\gamma_{\max} \approx 2.82 + \gamma_0$. By selecting γ_0 we set the background vorticity: $\gamma_0 = 0$ describes an isolated vortex, $\gamma_0 > 0$ a prograde (equally-signed) vortex, and $\gamma_0 < 0$, $\gamma_{\max} > 0$ a retrograde (oppositely-signed) vortex.



a) initial vortex density b) vortex at $\tau = 3$

Fig.8 Rollup of the Gaussian-distribution shear line.

Fig.8 shows the results at time $\tau = 3$ for γ_0 = 0, 0.5, and -0.5, satisfying the criteria for the above three types of flow. In the first frame we observe an isolated vortex nearing a fully developed stage; there is no more vorticity available to be rolled up. The prograde vortex in the second frame continues to grow indefinitely (although to a finite limit) by attracting and winding up the surrounding line of vorticity. The retrograde vortex in the third frame does not attract the shear line, but rather repudiates it. The oppositely-signed shear develops its own rollups at its ends. This behaviour is very similar to that observed previously: the equally-signed vorticity merges, the oppositely-signed vorticity does not.

Atmospheric shear is usually associated with the rollup of aircraft vortices [49] and faster decay. The latter, as several numerical simulation studies indicate, is only partially true. From the observed asymmetry of an aircraft vortex pair in ambient shear it appears that the prograde vortex is not only less susceptible to erosion than the retrograde vortex [50][51], but may even grow [52]-[54].

The discrete vortex sheet method can again be used to examine the inviscid mechanism of this growth. The picture sequence in Fig.9 shows a pair of counter-rotating vortices descending into a narrow shear band. The prograde vortex is seen to grow by winding the shear layer around itself while the retrograde vortex repels it. Admittedly, a number of other possibilities exist. For example, if the shear is weak, the vortices just break through and continue to descend, albeit with a changed slope [13].

The initial conditions of the case in Fig.9 are:
Wing trailing sheet (elliptic loading)

$$\gamma = 4\,(2x/b)[1 - (2x/b)^2]^{-1/2}, \quad |x|/b < 1/2,\ y/b = 0 \qquad (30)$$

Cross-wind shear

$$\gamma = -1.0, \quad -\infty < x/b < \infty, \quad y/b = -0.5 \qquad (31)$$

The wing-span averages of the absolute values of the vortex densities of Eqs.(30) and (31)

$$\frac{1}{b}\int_{-b/2}^{b/2} |\gamma(x)|dx = \begin{cases} 4, & \text{wing} \\ 1, & \text{shear} \end{cases}$$

can be used to relate the wake vortex strength to shear intensity.

https://doi.org/10.1017/S0001924000000531 Published online by Cambridge University Press

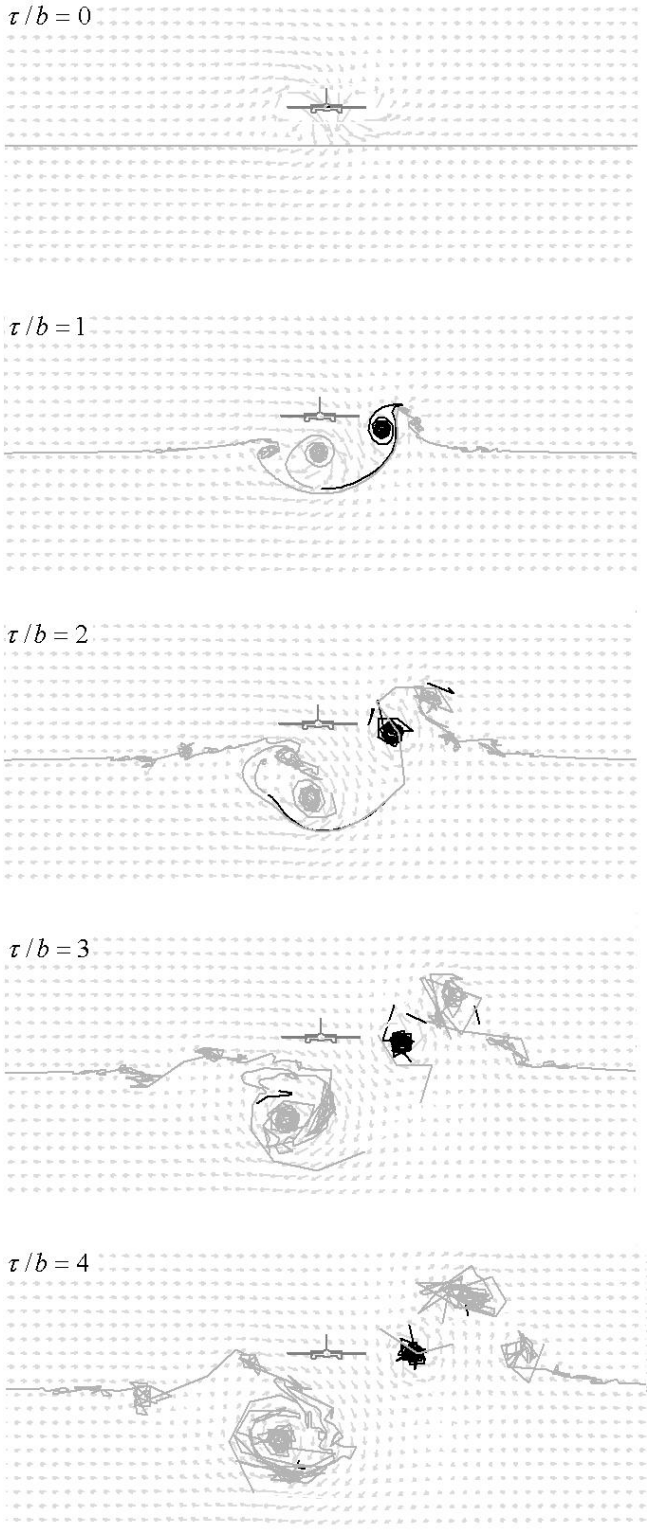


Fig.9 Vortex couple interacting with a line of shear.

Significant crosswind shear layers, where the possibility of shear-intensified vortices exists, are commonly associated with low-level jets. Although in some recent aircraft accidents initiated by wake vortex encounters the wind shear presence was noted, it was not considered as a contributing factor. A part of the problem is that a broad synoptic scale view of air flow may imply benign low-level wind shear conditions, when in actual fact local conditions may result in severe wind shears [55]. Besides the wind velocity gradient, the life cycle of aircraft vortices depends on the vertical temperature gradient and other atmospheric parameters [56]. Clearly, a lot of atmospheric research needs to be done to determine the balance of the shear-induced decay and possible wake vortex intensification.

The growth of a wake vortex in crosswind shear has not been observed experimentally yet, but its possibility is suggested by the existence of Kelvin-Helmholtz waves that form spontaneously along atmospheric shear layers. These periodically spaced roll-ups evolve from shearing instabilities when the Richardson number (ratio between stratification and shear forces) becomes sufficiently small. An encounter with a ”train” of wind shear vortices, quantified from the flight recorder data, has been reported in Ref.[57]. It is conceivable that if aircraft wake vortices are planted into a shear layer that is near Kelvin-Helmholtz unstable, the prograde vortex may become a nucleus of subsequent roll-up.

Among other phenomena closely related to the shear-intensified vortices are also the recently discovered Horizontal Vortex Tubes (HVT). These tubes, triggered by complex jet stream processes or high winds over mountainous terrain, can evolve into tornado-like structures and cause severe upsets to aircraft that fly into them [58][59].

Conclusions

It was demonstrated that the merger phenomenon plays a key role in the formation of aircraft vortices and their interactions with ambient shear. Numerical simulations are in a reasonable agreement with available experimental results and may thus be used as prediction when a relevant experiment is difficult to make. Although the fundamental mechanism of the merger process is known, it is a fairly complex phenomenon whose existence proof based on vorticity advection and conservation laws is yet to be given.

https://doi.org/10.1017/S0001924000000531 Published online by Cambridge University Press

References

[1] MEUNIER, P. and LEWEKE, T. Merging of a pair of corotating vortices, Album of Visualization, The Visualization Society of Japan, No.16, 1999, pp.1-2.

[2] LEITH C.E. Minimum enstrophy vortices, Phys. Fluids, Vol.27, No.6, 1984, pp.1386-1395.

[3] CHORIN, A. Vorticity and turbulence, Springer-Verlag, New York, 1994, pp.84-89.

[4] McWILLIAMS, J.C. The vortices of two-dimensional turbulence, J. Fluid Mech., Vol.219, 1990, pp.361-385.

[5] DRITSCHEL, D.G. Vortex properties of two-dimensional turbulence, Phys. Fluids A, Vol.5, 1993, pp.984-997.

[6] LANDER, M. and HOLLAND, G.J. On the interaction of tropical-cyclone-scale vortices. I: Observations, Quart. J. Roy. Met. Society, Vol.119, 1993, pp.1347-1361.

[7] PAVIA, E.G. and CUSHMAN-ROISIN, B. Merging of frontal eddies, J. Phys. Oceanography, Vol.20, 1990, pp.1886-1906.

[8] DRISCOLL, C.F., FINE, K.S. Experiments on vortex dynamics in pure electron plasmas, Phys. Fluids B, Vol.2, 1990, pp.1359-1368.

[9] FINE, K.S., DRISCOLL, C.F., MALMBERG, J.H., and MITCHELL, T.B. Measurements of symmetric vortex merger, Phys. Rev. Letters, Vol.67, No.5, 1991, pp.588-591.

[10] AMORETTI, M., DURKIN, D., FAJANS, J., POZZOLI, R., and ROMÉ M. Asymmetric vortex merger: experiments and simulations, Physics of Plasmas, Vol.8, No.9, 2001, pp.3865-3868. Vol.67, No.5, 1991, pp.588-591.

[11] MITCHELL, T.B. and DRISCOLL, C.F. Electron vortex orbits and merger, Phys. Fluids, Vol.8, 1996, pp.1828-1841.

[12] DRISCOLL, C.F., JIN, D.Z., SCHECTER, D.A., and DUBIN, D.H.E. Vortex dynamics of 2D electron plasmas, Physica C 369, 2002, pp.21-27.

[13] MOKRY, M. Numerical simulation of aircraft trailing vortices interacting with ambient shear or ground, J. Aircraft, Vol.38, No.4, 2001, pp.636-643.

[14] MUSKHELISHVILI, N.I. Singular integral equations, Noordhoff-Groningen, 1953, pp.42-43.

[15] RAFFEL, M., WILLERT, C.E., and KOMPENHANS, J. Particle image velocimetry - A practical guide, Springer-Verlag 1998, p.162.

[16] MELANDER, M.V., ZABUSKY, N.J., and McWILLIAMS, J.C. Symmetric vortex merger in two dimensions: Causes and conditions, J.Fluid Mech., Vol.195, 1988, pp.303-340.

[17] WAUGH, D.W. The efficiency of symmetric vortex merger, Phys. Fluids A Vol.4, No.8, 1992, pp.1745-1758.

[18] SHASHIKANTH, B.N. and NEWTON, P.K. Geometric phases for corotating vortex patches, J. Math. Phys., Vol.41, 2000, pp.8148-8162.

[19] MARSHALL, J.S. Inviscid incompressible flow, J. Wiley, New York, 2001, pp.186-191.

[20] ROBERTS, K.V. and CHRISTIANSEN, J.P. Topics in computational fluid mechanics, Comput. Phys. Commun., Vol.3, 1972, pp.14-32.

[21] CHRISTIANSEN, J.P. and ZABUSKY, N.J. Instability, coalescence and fission of finite-area vortex structures, J. Fluid Mech., Vol.61, 1973, pp. 219-243.

[22] ZABUSKY, N.J., HUGHES, M.H., ROBERTS, K.V. Contour dynamics for the Euler equations in two dimensions, J. Comp. Phys., 1979, Vol.30, pp.96-106.

[23] DRITSCHEL, D.G. Contour dynamics and contour surgery, Computer Physics Reports, 1989, Vol.10, pp.77-146.

[24] PULLIN, D.I. Contour dynamics methods, Annu. Rev. Fluid Mech, Vol.24, 1992, pp.89-115.

[25] ROSSOW, V.J. Convective merging of vortex cores in lift-generated wakes, J. Aircraft, Vol.14, No.3, 1977, pp.283-290.

[26] MOORE, D.W. The stability of an evolving two-dimensional vortex sheet, Mathematika, Vol.23, 1976, pp.35-44.

[27] DRITSCHEL, D.G. On the stabilization of a two-dimensional vortex strip in adverse shear, J. Fluid. Mech., Vol 206, 1989, pp.193-221.

[28] CROW, S. Stability theory for a pair of trailing vortices, AIAA J. Aircraft, Vol.8, No.12, 1970, pp.2172-2179.

[29] LEWEKE, T. and WILLIAMSON, C.H.K. Cooperative elliptic instability of a vortex pair, J.Fluid Mech., Vol.360, 1998, pp.85-119.

[30] MELESHKO, V.V. and VAN HEIJST, G.J.F. Interacting two-dimensional vortex structures: point vortices, contour kinematics and stirring properties, Chaos, Solitons & Fractals, Vol.4, 1994, pp.977-1010.

[31] DRITSCHEL, D.G. The nonlinear evolution of rotating configurations of uniform vorticity, J.Fluid Mech., Vol.172, 1986, p.157-182.

[32] GRIFFITHS, R.W. and HOPFINGER, E.J. Coa-

https://doi.org/10.1017/S0001924000000531 Published online by Cambridge University Press

lescing of geostropic vortices, J. Fluid Mech., Vol.178, 1987, pp.73-97.

[33] CHEN, A.L., JACOB, J.D., and SAVAS, Ö. Dynamics of corotating vortex pairs in the wakes of flapped airfoils, J. Fluid Mech., Vol.382, 1999, pp.155-193.

[34] LI, X. and JACOB, J.D. Initial spacing effects on co-rotating tip vortex formation and merger, AIAA 2000-2219, Fluids 2000.

[35] DRITSCHEL, D.G. and WAUGH, D.W. Quantification of the inelastic interaction of unequal vortices in two-dimensional vortex dynamics, Phys. Fluids A Vol.4, No.8, 1992, pp.1737-1744.

[36] MELANDER, M.V., ZABUSKY, N.J., and McWILLIAMS J.C. Asymmetric vortex merger in two dimensions: Which vortex is victorious? Phys. Fluids, Vol.30, 1987, pp.2610-2612.

[37] DRITSCHEL, D.G. A general theory for two-dimensional vortex interactions, J. Fluid Mech., Vol.293, 1995, pp.269-303.

[38] HUENECKE, K. and HUENECKE C. Flowfield visualization in aircraft wake vortex research, 9th International Symp. on Flow Visualization, Paper 139, Edinburgh, UK, 2000.

[39] JACQUIN, L., FABRE, D., and GEFFROY, P. The properties of a transport aircraft wake in the extended near field: an experimental study, AIAA 2001-1038, 39th AIAA Aero. Sci. Meeting, Reno, NV, 2001.

[40] ALBANO, F., DE GREGORIO F., and RAGNI, A. Trailing vortex detection and quantitative evaluation of vortex characteristics by PIV technique, Paper 2.2,20th Intern. Congress on Instrum. in Aerospace Simulation Facilities, Göttingen, Germany, 2003.

[41] STUMPF, E., HEPPERLE, M., DARRACQ, D., MEESE, E.A., ELPHICK, G., and GALPIN, S. Benchmark test for Euler calculations of a high lift configuration vortex wake, AIAA-2002-0554, 40th Aerospace Sci. Meeting & Exhibit, Reno, NV, 2002.

[42] GRAHAM, W. R., PARK, S.W., and NICKELS, T.B. Trailing vortices from a wing with a notched lift distribution, AIAA J., Vol.41, No.9, 2003, pp. 1835-1838.

[43] CORSIGLIA, V.R., IVERSEN, J.D., and ORLOFF, K.L. Laser-velocimeter surveys of merging vortices in a wind tunnel, J. Aircraft, Vol.15, 1978, pp.762-768.

[44] BREITSAMTER, C., BELLASTRADA, C., and LASCHKA, B. Investigations on the turbulent wake vortex flow of large transport aircraft, ICAS Congress, 2002, pp.382.1-382.13.

[45] CLIFFONE, D.L. Vortex interactions in multiple vortex wakes behind aircraft, J. Aircraft, Vol.14, 1977, pp.440-446.

[46] BAO, F., VOLLMERS, H. and MATTNER, H. Experimental study on controlling wake vortex in water towing tank, ICIASF'03, 2003, pp.214-223.

[47] VELDHUIS, L.L.M., SCARANO F., and VAN WIJK, C. Vortex wake investigation of an Airbus A340 model using PIV and towing tank, AIAA 2003-3814, Appl. Aero. Conference, Orlando, 2003.

[48] GRAHAM, W. R. Optimising wing lift distribution to minimize wake vortex hazard, Aeronautical J., Vol.106, 2002, pp.413-426.

[49] TOMBACH, I. Observation of atmospheric effects on vortex wake behavior, J. Aircraft, Vol.10, 1973, pp.641-647.

[50] BILANIN, A.J., TESKE, M.E., and HIRSCH, J.E. Neutral atmospheric effects on the dissipation of aircraft vortex wakes, AIAA J., Vol.16, 1978, pp.956-961.

[51] ROBINS R.E. and DELISI, D.P. Numerical study of vertical shear and stratification effects on the evolution of a vortex pair, AIAA J., Vol.28, 1990, pp.661-669.

[52] LEWELLEN, D.C. and LEWELLEN, W.S. Large-eddy simulations of the vortex-pair breakup in aircraft wakes, AIAA J., Vol.34, 1996, pp.2337-2345.

[53] GARTEN, J.F., ARENDT, S., FRITTS, D.C., and WERNE, J. Dynamics of counter-rotating vortex pairs in stratified and sheared environments, J.Fluid Mech., Vol.361, 1998, pp.189-236.

[54] MOKRY, M. Intensification of aircraft wake vortices in crosswind shear, J. Aircraft, Vol.40, No.2, 2003, pp.405-407.

[55] FICHTL, G.H., CAMP, D.W., and FROST, W. Sources of low-level wind shear around airports, J. Aircraft, Vol.14, No.1, 1977, pp.5-14.

[56] FRECH, M. and ZINNER, T. Concept of wake vortex behavior classes, J. Aircraft, Vol.41, No.3, 2004, pp.564-570.

[57] BROWN, A.P., POLITIS, E. and OTHMAN, A. Line vortex modelling of vortices encountered as takeoff windshear by widebody jet transport, AIAA-2003-5384, AIAA Atm. Flight Mech. Conference, Austin, TX, 2003.

[58] CLARK, T.L., HALL, W.D., KERR, R.M., MIDDLETON, D., RADKE, L.F., RALPH, F.M., NEIMAN, P.J., and LEVINSON, D. Origins of aircraft-damaging clear-air turbulence during the 9 December 1992 Colorado downslope windstorm: Numerical simulations

https://doi.org/10.1017/S0001924000000531 Published online by Cambridge University Press

and comparison with observations, J. Atmospheric Sci., Vol.57, 2000, pp.1105-11.

[59] CLARK, T.L. and RADKE, L.F. Horizontal vortex tubes, clear air turbulence and implications for aviation safety, to be published in ICAO J.

https://doi.org/10.1017/S0001924000000531 Published online by Cambridge University Press